DEPARTMENT OF THE INTERIOR
U.S. GEOLOGICAL SURVEY

An analysis of a Unique Seismic Anomaly in Georges Bank Basin, Atlantic Continental Margin

by

M.W. Lee[1], W.F. Agena[1], and B.A. Swift[2]

U.S. Geological Survey
Open-File Report 91-138

[1] U.S. Geological Survey, Box 25046, Denver Federal Center, Denver, CO 80225
[2] U.S. Geological Survey, Woods Hole, MA 02543

1991

Table of Contents

Table of Figures

Table of Tables

An Analysis of a Unique Seismic Anomaly in Georges Bank Basin, Atlantic Continental Margin

M.W. Lee, W.F. Agena, and B.A. Swift

Abstract

A high-amplitude anomaly observed on a seismic line shot over the Georges Bank Basin, southeast of New England, is unique in shape and magnitude. The anomaly is encased by Jurassic evaporites at a depth of about 4200 m over the basement of lower Paleozoic crystalline rocks. In 1981, Exxon drilled this structure where a salt layer had been inferred for this anomalous interval. The main purpose of this investigation has been to analyze this seismic anomaly in detail and to assess our ability to define the anomaly in terms of lithology using only surface seismic profile data together with our geologic knowledge of this area.

The analysis was performed using wavelet, and true-amplitude (TA) processed seismic profiles of USGS line 12 and the results were compared to well log information. The center of the 9 km wide anomaly consists of two prominent troughs with a separation of about 60 ms. Both edges of the anomaly are characterized by higher peak amplitudes with diffractions.

Seismic analysis indicates that the 130m thick anomalous zone consists of low impedance layers with an interval velocity in the range of 4 km/s and an apparent reflection coefficient for the top of the anomalous zone of about -0.18. Our preferred interpretation of this anomalous zone is a salt intrusion surrounded by acoustically homogeneous limestone and other evaporites.

Introduction

During the 1970's, the U.S. Geological Survey (USGS) collected more than 50 multichannel seismic reflection profiles across the Atlantic continental shelf and rise. One of these profiles, a strike line 12, crosses the northernmost part of the Georges Bank basin (Figure 1), and exhibits a high-amplitude seismic anomaly extending laterally approximately 9 km at a depth of around 4200 m.

This anomaly has been investigated previously by Anderson and Taylor (1981) and they suggested that the anomalous zone can be best correlated with low-impedance layers, either a salt lens or some combination of porous carbonates. Their analysis was based on two-dimensional seismic modeling and somewhat ambiguous polarity information in conjunction with regional geology.

Because of commercial interest and possible gas accumulation, Exxon drilled this anomaly in 1981. Samples taken from OCS153A (EX971-1) infer that the anomalous interval is a salt layer surrounded by other evaporites and limestone.

The purpose of this investigation was to see whether we could make a reasonable lithological interpretation of the anomaly based solely on the observed surface seismic data and general geology of the area. In other words, we wanted to see if analysis from current reflection seismic technology could have inferred the lithological information before drilling.

One current method used in delineating lithologies from the seismic data is through the use of amplitude versus offset (AVO) analysis (Backus, 1987). However, the lack of the source and geophone array information, the non-uniform channel sensitivity, and very noisy far-offset data precluded AVO analysis for this data set. Thus, our analysis is based mainly on the stacked seismic data.

To get clear polarity and amplitude information from the recorded seismic data, we applied both wavelet deconvolution and true amplitude (TA) processing. All seismic information was

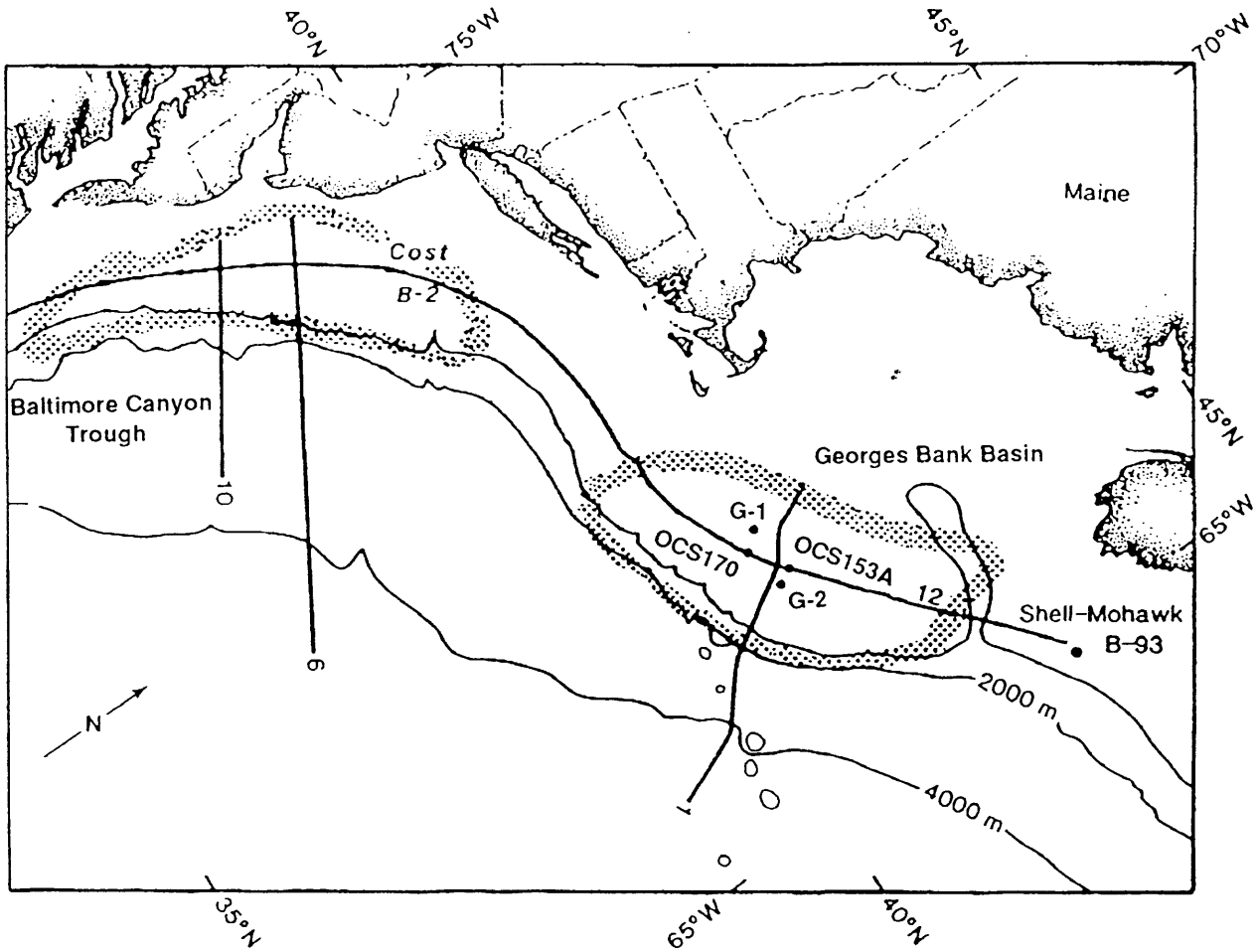

Fig. 1 Location map of study area, seismic-reflection profiles, deep stratigraphic test wells and the OCS153A (EX975-1) well. The boundaries of Georges Bank Basin and the Baltimore Canyon Trough are outlined by dots (Modified from Anderson and Taylor, 1981).

cross-checked with available well data.

The center of the anomalous zone is characterized by prominent wavelet troughs at the top and the bottom separated by two small peaks. Constructive wavelet interference and diffractions are manifested toward the edge of the anomaly. The apparent reflection coefficient for the anomaly is in the range of -0.18 and its thickness is about 130 m. Based on the result of seismic inversion and the mapping of the time delay associated with this anomaly, the interval velocity is approximately 4 km/s, which is close to the velocity obtained from well log analysis. However, the seismic expression based on the sonic data differs from the observed seismic anomaly and we offer an explanation for this discrepancy.

Based on the draping of the upper horizons over the anomaly and the total time delay associated with this anomaly, we interpret this anomalous feature as a salt intrusion, possibly derived from the salt deposited over the basement rock.

Geologic setting

Georges Bank is a shallow part of the Atlantic Continental Shelf southeast of New England (Emery and Uchupi, 1972) and covers several small sedimentary sub-basins overlying a block-faulted basement of igneous and metamorphic crystalline rock (Figure 2). Georges Bank Basin contains sediments in some areas more than 10 km thick. Basement platforms adjoining the basin to the northeast and southwest contain sediments less than 5 km thick.

Mattick and others (1975) suggested that the shelf edge acted as a barrier to the Atlantic circulation system during Triassic time and established a shallow, restricted marine environment in the Georges Bank Basin. Sedimentation up through the Middle Jurassic probably occurred in a less restricted yet relatively shallow marine environment, parts of which could have been above the sea level necessary for the formation of evaporites. Schlee and others (1976, 1977) hypothesized that thick accumulation of limestone, dolomite, and anhydrite may have formed in the central basin regions in Middle Jurassic time.

The presence of a Jurassic salt layer throughout the Scotian Shelf and Grand Banks was reported by Sherwin (1973) and Jansa and Wade (1975). Swift (written communication, 1991), based on the work of Poag and Sevon (1989), hypothesized that the Early Jurassic Baltimore Canyon Trough was a small and restricted basin like Georges Bank where an arid, possibly semi-arid, paleoclimate could have created the hypersaline conditions necessary for salt deposition. Thus, evaporites including salt could have been deposited over basement during the Jurassic time in the Georges Bank Basin.

Data Acquisition and Processing

This data set was acquired by DIGICON Geophysical Corp. in 1975. Using a 3848m long cable with 48 non-linearly spaced hydrophone groups, and shotpoint intervals of 100m enabled us to obtain 48-fold common midpoint(CMP) coverage, although the data were originally processed at 36-fold. A tuned airgun array totalling 1700in^3 was the seismic source. Analysis during processing noted that channel sensitivity was highly variable and the far-24 traces were heavily contaminated by noise.

Two processing sequences were performed on the data. The first sequence, shown in the left hand column of Table 1, followed conventional automatic gain control (AGC) methods and will be noted as AGC processing throughout this paper. This first pass was used to allow us to get detailed structural information and to optimize processing parameters. For the second processing sequence, shown in the right-hand column of Table 1, care was taken to preserve the true amplitude of the data as much as possible and it will be noted throughout this paper as TA processing. Notable differences from the first sequence include the systematic corrections for amplitude

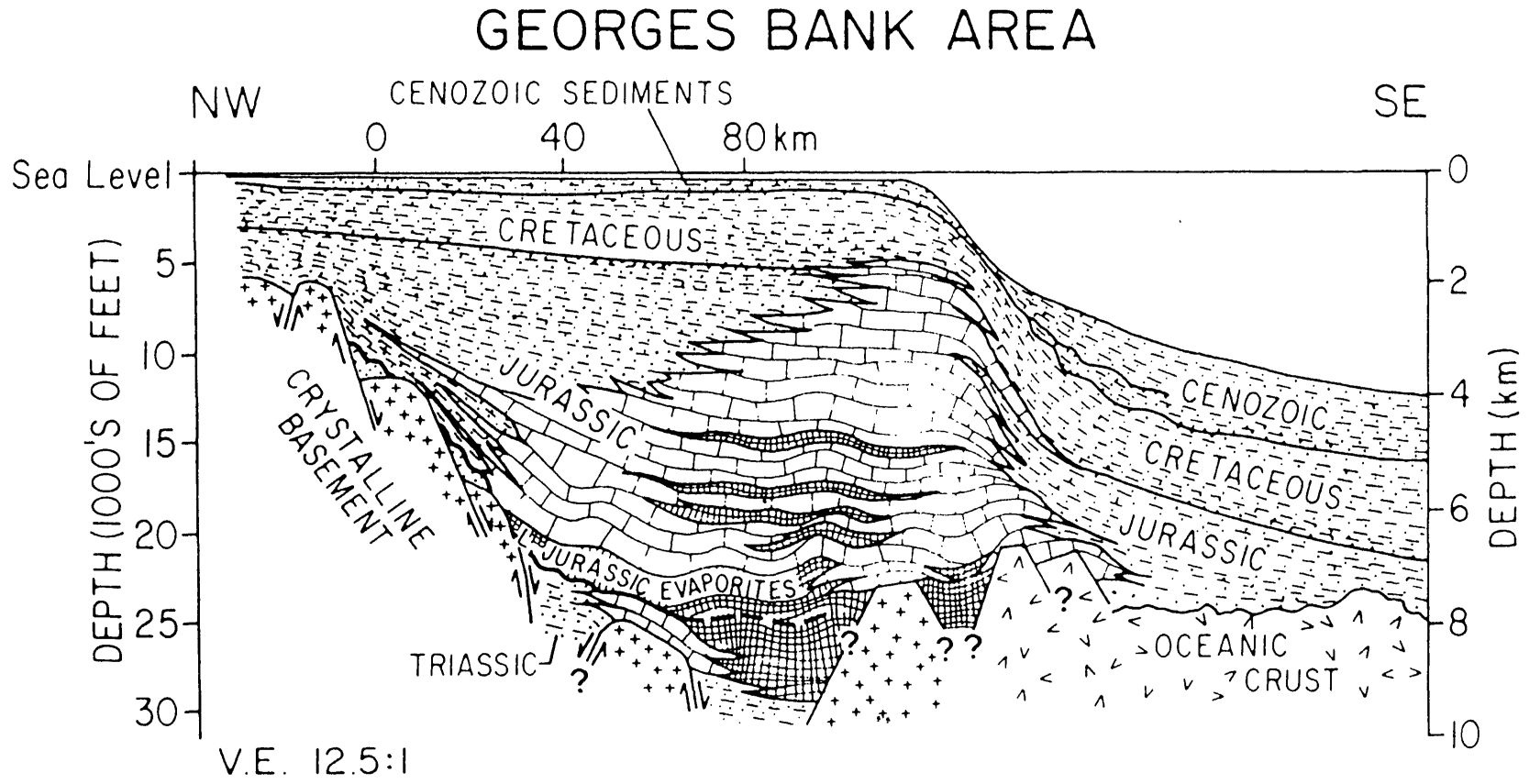

Fig. 2 Schematic cross-section through Georges Bank Basin, showing the distribution of the sedimentary wedge bounded by the seafloor and crystalline basement (from Schlee and Klitgord, 1981)

decay, the wavelet deconvolution, and automated editing of noisy traces. An example of amplitude decay for CMP 460 is shown in Figure 3. We used $T^{1.93}$ as a correction for the amplitude decay for this profile. For the wavelet deconvolution we used a variable norm method (Gray, 1979)

Conventional Processing Flow ("**AGC**" - Processing)	**True Amplitude Processing Flow** ("**TA**" - Processing)
Demultiplex	Demultiplex
Geometry	Geometry
Sort	Sort
Resample (4.0ms)	Resample (4.0ms)
Deconvolution (Spiking)	**Deconvolution (Wavelet)
AGC	**Correct for Spherical Divergence & Attenuation Loss
Normal Moveout	Normal Moveout
Mute	Mute
Bandpass Filtering	**Automatic Trace Editing
Stack (48-Fold)	Stack (48-Fold)
Deconvolution (Predictive)	Deconvolution (Predictive)
Time-Variant Filtering	Time-Variant Filtering
Display	Display

Table 1. Two processing sequences (AGC and TA) used for the investigation of the anomalous zone shown over USGS seismic profile 12 near Georges Bank Basin. The major processing differences beween AGC and TA are denoted as ** in the TA processing sequence.

to estimate the source wavelet which was then used to design and apply an inverse filter. But, due to the extremely shallow water depth in the study area, we could not extract a wavelet from this line. Thus, we extracted a source wavelet from the deep water section of line 6 which was acquired with identical field parameters. The validity of this approach is justified by the good match beween synthetic seismograms created from well log data and the actual recorded surface seismic data which will be discussed later. Careful filtering and instrument monitoring during the

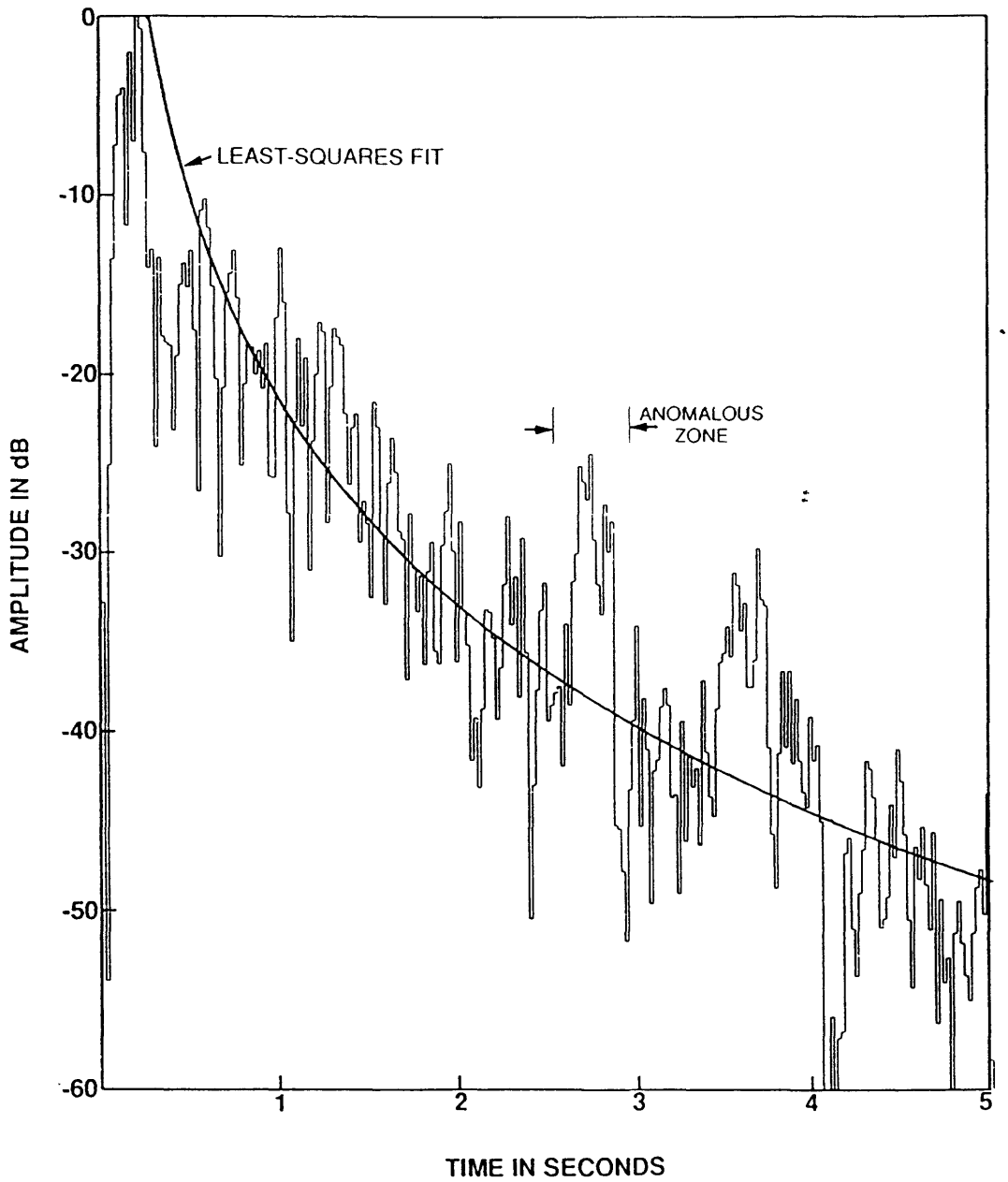

Fig. 3 Amplitude decay analysis of CMP gather 460 of line 12. The heavy solid line represents a least-squares fit curve, proportional to $T^{-1.93}$ where T is two-way travel time. The anomalous amplitude is about 12 db higher than amplitudes of the surrounding background reflections.

acquisition of the data usually eliminates time variant noise bursts. However, lateral noise variations are more difficult to handle. These variations, recorded in the time-offset (T-X) domain can be caused by actual variations in the earth's response, or by changes in recording conditions often caused by the loss of one or more guns in the source array. To filter out lateral variations caused by artifacts, we implemented an automatic editing algorithm developed by Lee and Hutchinson (1990).

Well Log Analysis

A variety of geophysical well logs were run on OCS153A (EX971-1) and a few logs for the interval beteen 12500 ft and 14600 ft are shown in Figure 4. The sample descriptions for the interval show siltstone and sandstone at the top, with interlayered limestone and anhydrite at the depths at which salt is inferred from chloride levels. Below, there is a sandstone (14000 ft) and shale (14100 ft) underlain by limestone and anhydrite. The huge wash-out zone between 13800 ft and 14125 ft is due to the dissolution of salt. The gamma ray log indicates a shaly section between 14050 ft and 14100 ft. All of the log shapes are consistant with each other except for the formation compensation neutron log (FNCL), which differs from the others near 14000 ft. This difference implies that the log values within this anomalous interval are questionable.

Due to the large washout, the borehole compensated sonic and density logs may be in error in this interval. The cross plot between sonic and density log values for the interval shown in Figure 4 is shown in Figure 5. The high interval velocity above and below the anomalous zone is either dolomite, limestone or anhydite, which corresponds well to the lithlogical description and inferred porosity, which based on this cross-plot, is less than about 15%.

The area shown as salt in Figure 5 fits the actual sonic and density point for this anomalous interval, although the density of 2.02 gr/cc is less than usual salt density of 2.2 gr/cc. Overall the acoustic properties for the entire interval below 12500 ft fit the lithological description rather well, but details of the acoustic properties for the anomalous zone are questionable.

The check shot data, shown in Table 2, indicate that the interval velocity between 14023 ft and 14267 ft (Between **B** and **C** in figure 4) is 20300 ft/s (6187 m/s), and 19200 ft/s (5852 m/s) for the interval between 14267 ft and 14517 ft (Between **C** and **D** in figure 4). This differs greatly from the sonic log and the consequence of this discrepancy will be addressed later. Check shot velocities for other intervals seem to match the sonic log. The average interval velocity of the upper part of the anomalous zone is about 4 km/s. Because of the huge wash-out, we suspect that the actual magnitude of sonic and density values within the anomalous zone, particularly for the lower anomalous zone, are in error.

Synthetics

In order to identify the key reflecting horizons, a synthetic vertical seismic profile (VSP) was generated using sonic log and check shot data. We did not use density information because of the inferior quality of the density log. In order to relate the seismic amplitude more directly to the depth, a synthetic VSP as well as a conventional synthetic seismogram were generated and are shown in Figure 6.

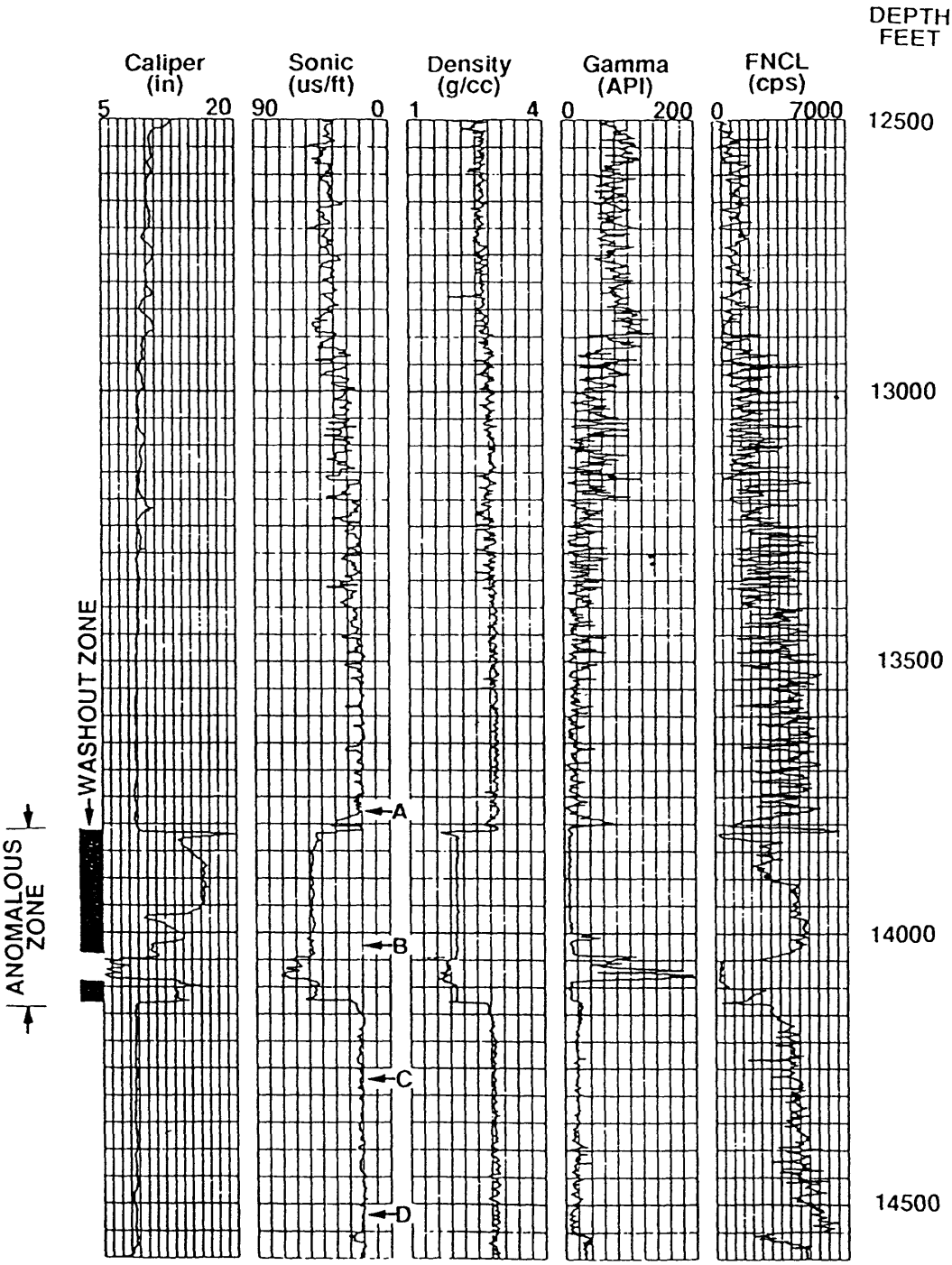

Fig. 4 Examples of the well logs at OCS153A (EX975-1) well for the anomalous interval. Note the huge washout zones in the caliper log. The interval velocities derived from the check shot data are 13500 ft/s, 20300 ft/s, and 19200 ft/s respectively for the intervals **A-B**, **B-C**, and **C-D**.

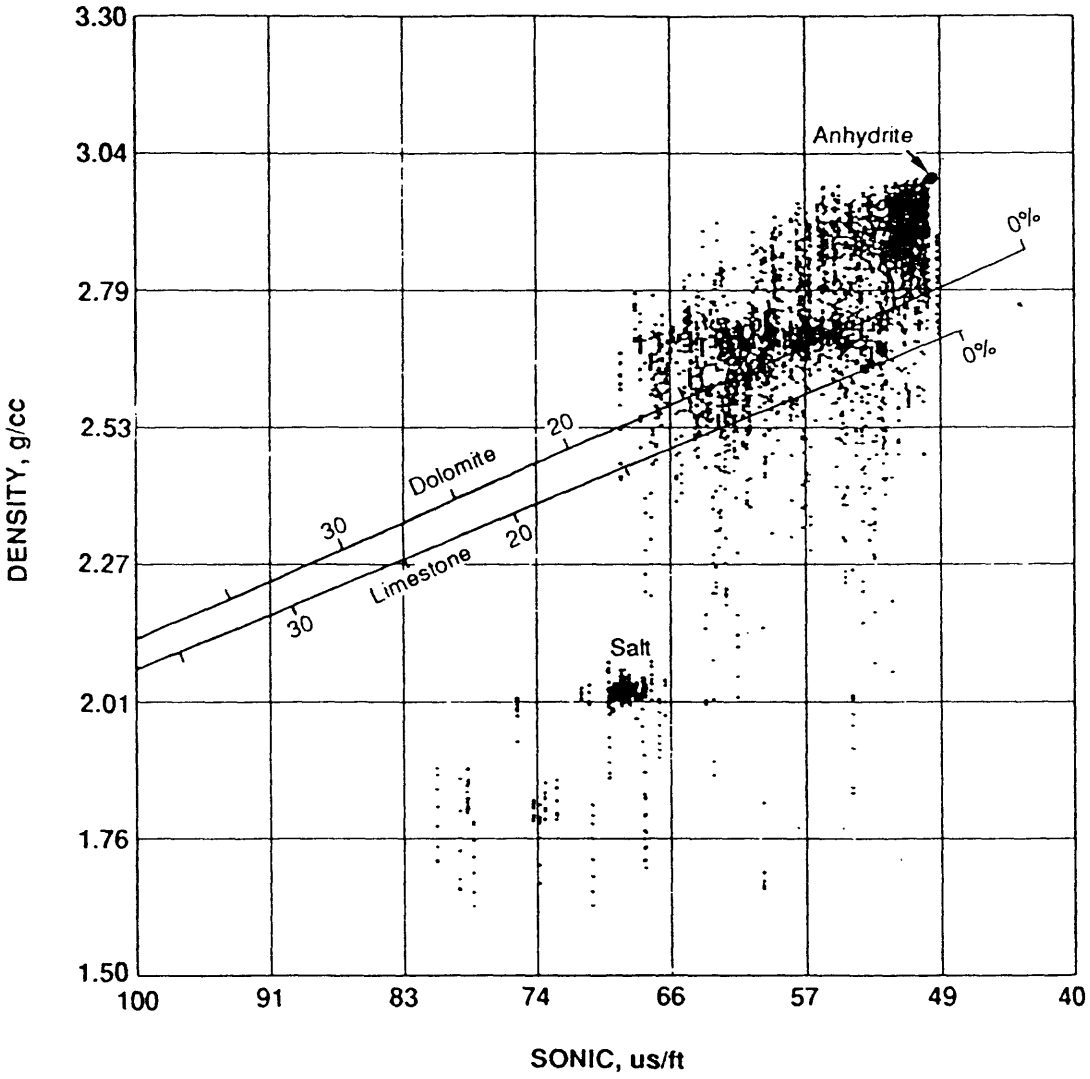

Fig. 5 Cross-plot of sonic and density log values from OCS153A (EX925-1) for the interval of 12,000 to 14,600 feet with some typical lithologies in this well. The number shown above the Dolomite or below the Limestone line indicates the porosity values.

Depth (feet)	One-way traveltime (ms)
0.0	0.0
2316.93	382.00
3017.06	461.00
3517.06	519.00
4017.06	574.00
4416.99	618.00
4916.99	668.00
5416.99	716.00
5916.99	757.00
6416.99	797.00
6916.99	844.00
7416.99	884.00
7816.93	917.00
8416.99	964.00
8916.99	1000.00
9416.99	1039.00
9916.99	1073.00
10416.99	1109.00
10916.99	1143.00
11416.99	1177.00
11916.99	1206.00
12276.90	1228.00
12517.06	1245.00
12756.89	1261.00
13017.06	1274.00
13267.06	1288.00
13517.06	1302.00
13766.40	1316.00
14023.62	1335.00
14267.06	1347.00
14517.06	1360.00

Table 2. Checkshot data from well OCS153A (EX975-1)

The synthetic VSP and accompanying synthetic seismograms for the OCS153A (EX975-1) well used the following procedure:

1) Interval transit times digitized at 0.5 ft sampling interval were edited to remove abnormally high or low velocities, and converted to equal time with one-way sampling interval of 1 ms.
2) Check shot information was incorporated into the two-way travel time computation, but actual sonic values were not corrected. This means that only two-way travel time versus depth is corrected by the check shot data. Other methods of compensating the sonic log with check shot data will be discussed later.
3) The total wave field, including all interbed multiples using the method outlined by Wyatt (1981), both upward (reflected)- and downward (transmitted)- travelling waves, was calculated at 100 ft depth intervals. The synthetic VSPs were then band pass filtered at frequency values ranging from 6/10-42/56 Hz.

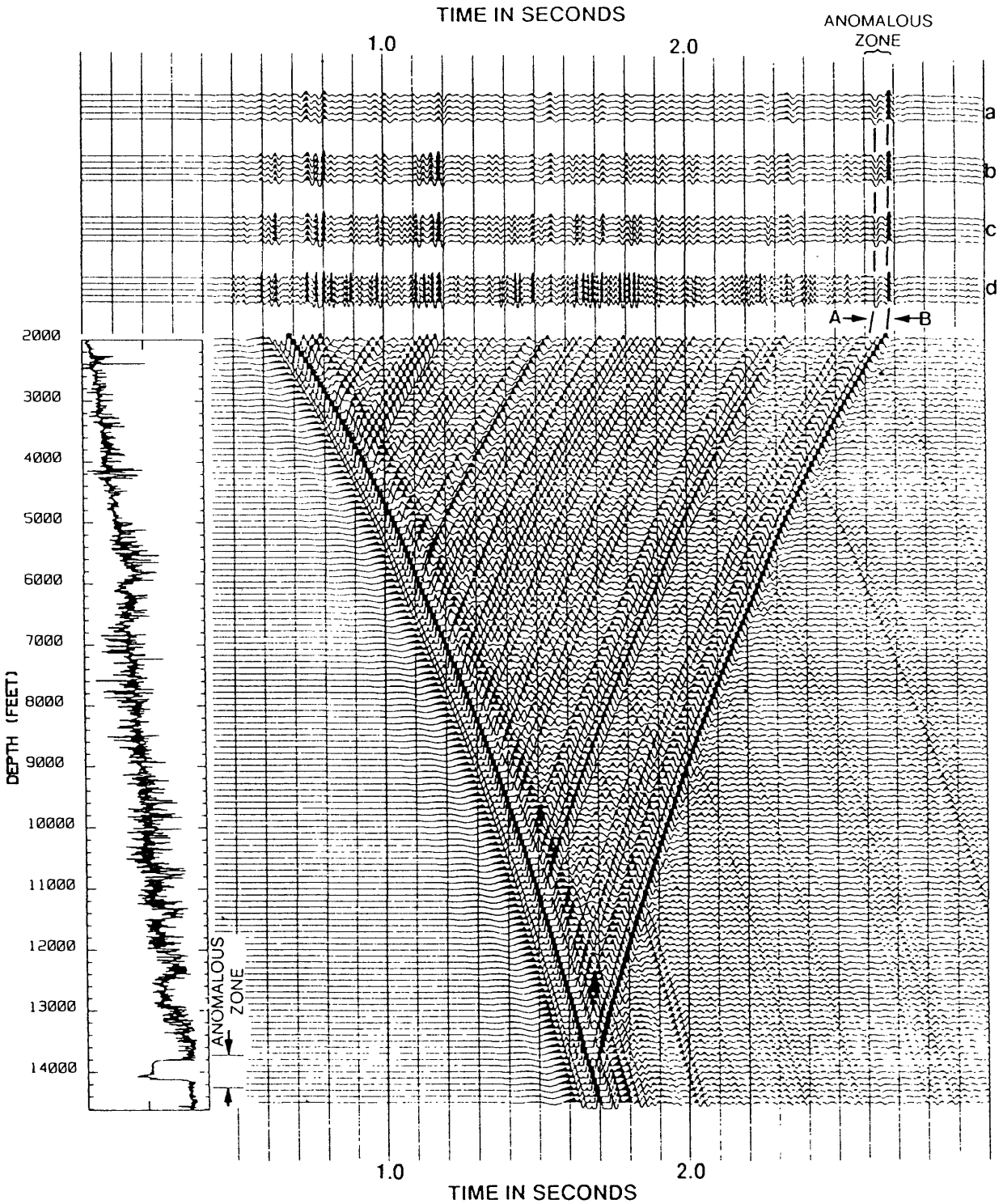

Fig. 6 Synthetic vertical seismic profile (VSP) with 6/10-42/56 Hz band-pass filter for the OCS153A (EX925-1) well. The top 4 figures are synthetic seismograms (a, b, c, and d) bandpass filtered at 6/10-42/56 Hz, 6/10-42/56 Hz, 6/10-50/68 Hz, and 6/10-68/96 Hz respectively. The letter **A** indicates the top of the anomaly and **B** the bottom. A velocity log is plotted alongside the VSP.

4) The resultant synthetic VSP was plotted using depth as the vertical axis and time as the horizontal axis. Synthetic seismograms recorded at the surface were plotted at the top of the figure with 4 different band pass filters (6/10-68/96, 6/10-50/68, 6/10-42/56, and 6/10-32/42 Hz) applied. Normal polarity, where a peak waveform results from a unit of low acoustic impedance layer overlying a unit of higher acoustic impedance, is maintained in all the plots except reverse polarity plots in Figures 11 and 12.

The broad peak (deflection to the right) before the large trough (deflection to the left), indicated as **A** in Figure 6, is the seismic response of the overlying evaporites and limestones. The anomalous zone is indicated as a large trough - peak combination separated by a small peak. Note that this configuration is present irrespective of the frequency content used.

The synthetic VSP clearly shows that the large trough, **A** in Figure 6, is generated at the upper boundary of the anomalous zone, where a sharp decrease in interval velocity is indicated in the accompanying velocity log and the peak, indicated as **B** in Fig 6, is the seismic response at the bottom of the anomalous zone characterized by the sharp increase in velocity. It appears that the interval between the top and bottom of the anomalous zone is seismically homogeneous. In other words, the anomalous zone in the synthetics is characterized by a trough-peak combination separated by approximately 50 ms.

Interpretation

A synthetic seismogram with band pass filtering (6/10 - 32/40 Hz) was inserted into the wavelet and TA processed seismic profile in order to correlate the reflecting horizons and to identify the anomalous interval (Figure 7). This figure indicates a good correlation between actual recorded seismic data and synthetic data. In particular, the broad peak preceeding the anomaly (about 2600 ms at the well site) is well correlated in shape and amplitude. However, fine details of the anomalous zone are quite different. The actual recorded seismic data indicate a trough-peak-trough combination instead of the trough-peak combination shown on the synthetic seismogram.

As mentioned previously, we suspected that the details of the sonic log in the anomalous zone may be inaccurate and its values are different from the check shot data. In order to examine the possibility of the erroneous sonic value, we applied a check shot correction to the sonic log itself. There are numerous means of altering the sonic log to fit the observed check shot data and some of the examples are shown in Figure 8. Detailed descriptions of the various correction methods are given in a users manual written for CoginiSeis Development's Digital Log Processing System (Macknight and Pena, 1988). The synthetic VSP based on a linear correction, is shown in Figure 9. The waveform of the synthetic seismogram based on the altered sonic log correlates more closely with actual seismic data. Unfortunately, the interval velocty indicated in Figure 9 is too high for the lithology identified from the well data. This high-velocity layer is an artifact due to forcing the sonic log to fit the check shot data by linear interpolation. The strong peak in Figure 9 around 2500 ms two-way travel time is also an artifact from the linear correction of the sonic log. These artifacts imply that we have to be careful in correcting the sonic data with the check shot data. In spite of this problem, the bettter correlation for the anomalous interval with new synthetic VSP (Fig. 9) suggests that the anomalous zone may contain a high-impedance layer.

This example presents a dilemma. Which of the two seismograms shown in Figures 7 and 9 is more reliable, and which is more accurate, the synthetic data or actual recorded seismic data? It is our interpretation that the actual seismic data are more accurate than the synthetic data and we believe that the sonic and density logs shown in Figure 4 for the anomalous interval contain erroneous values. The validity of our interpretation will be discussed later.

The top of the anomalous zone is characterized by troughs in both the synthetic and actual

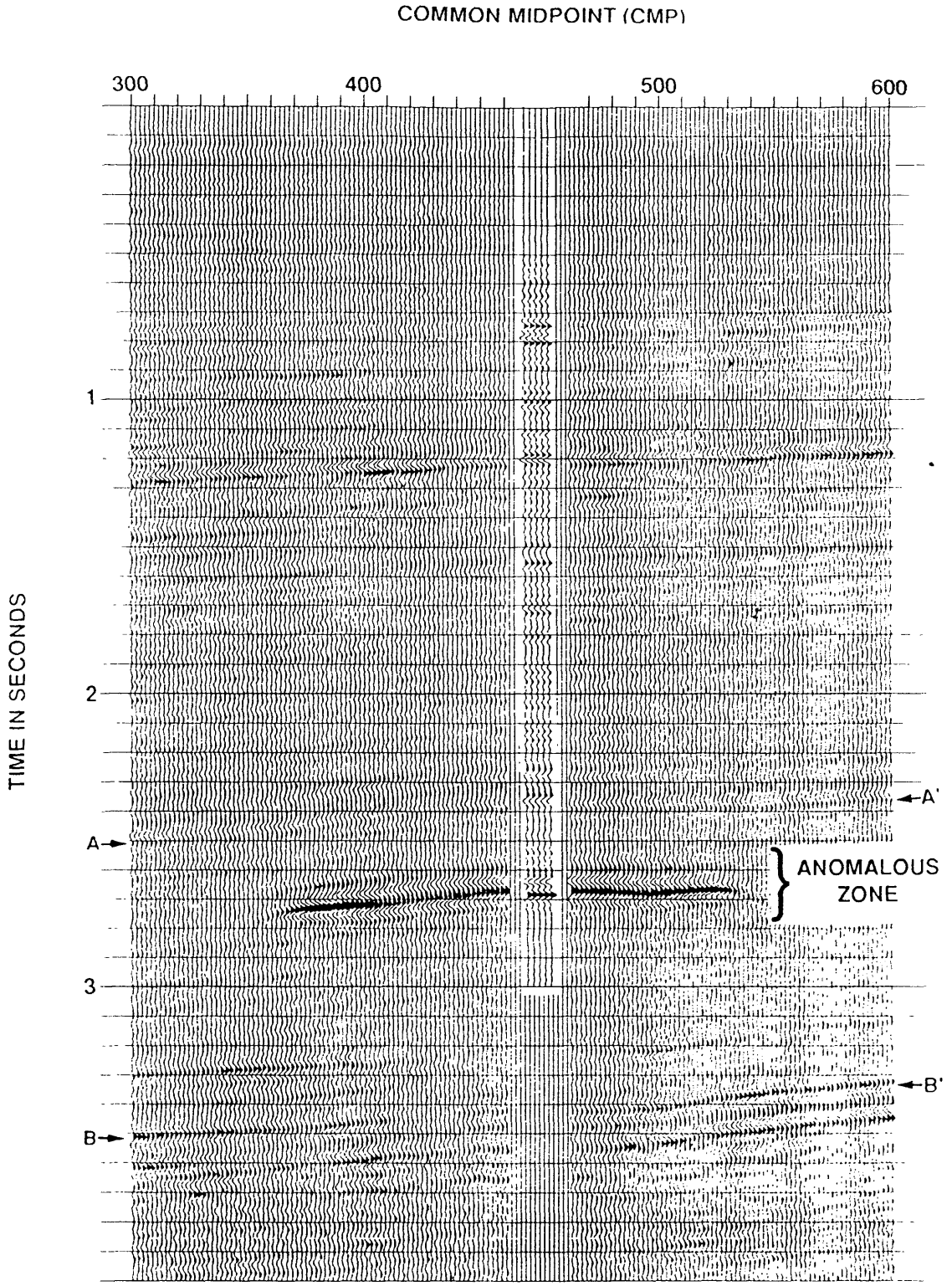

Fig. 7 True-amplitude and wavelet processed section over the anomaly with a synthetic seismogram inserted at the well location. Note the draping of horizons **A-A'** above the anomaly and the time sag of horizon **B-B'** below the anomaly.

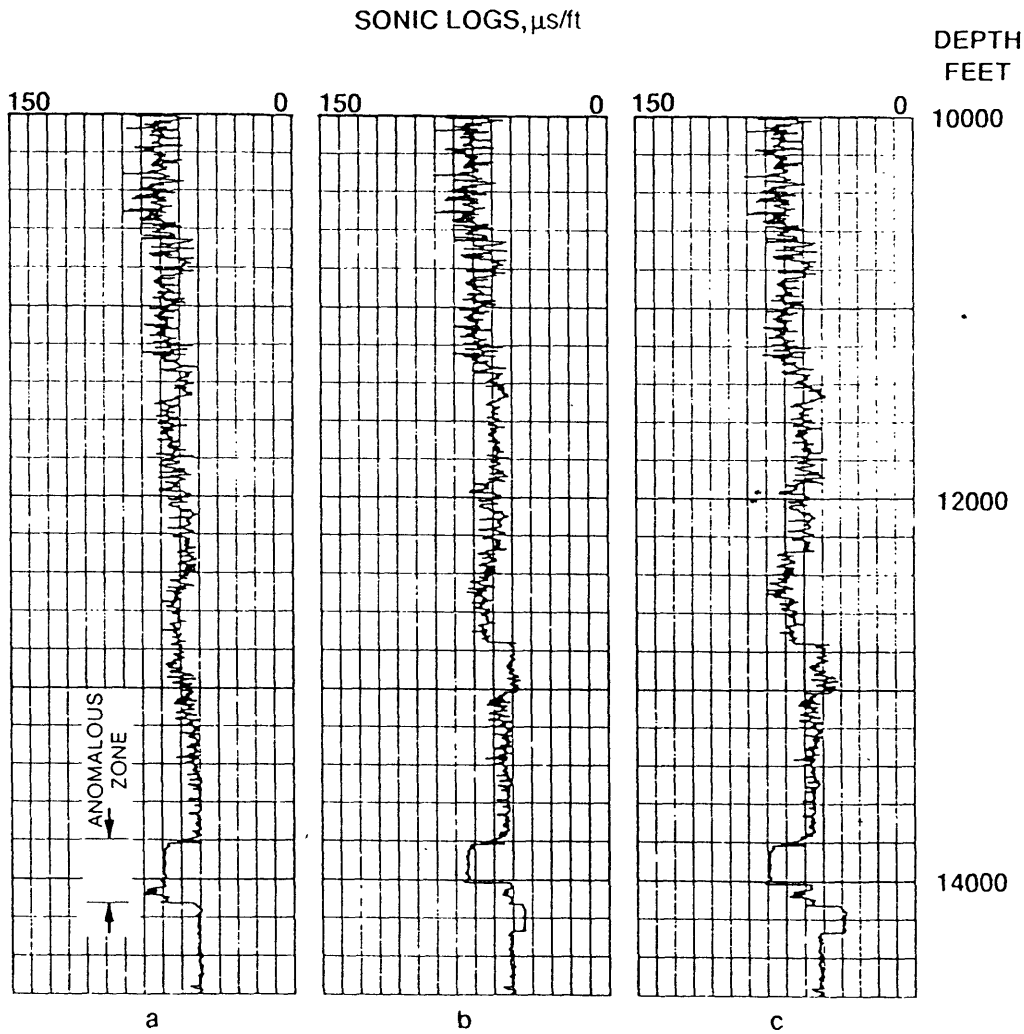

Fig. 8 Examples of the sonic log altered to fit the checkshot data. The large excursions at the checkshot data points (see table 2) are artifacts which generate erroneous amplitudes in the synthetic seismograms.

a) Original uncorrected sonic log

b) Corrected sonic log using a differential correction where a negative drift exists and a uniform correction where there are positive drift values.

c) Corrected sonic log using a straight linear fit, thus honoring the checkshot data exactly.

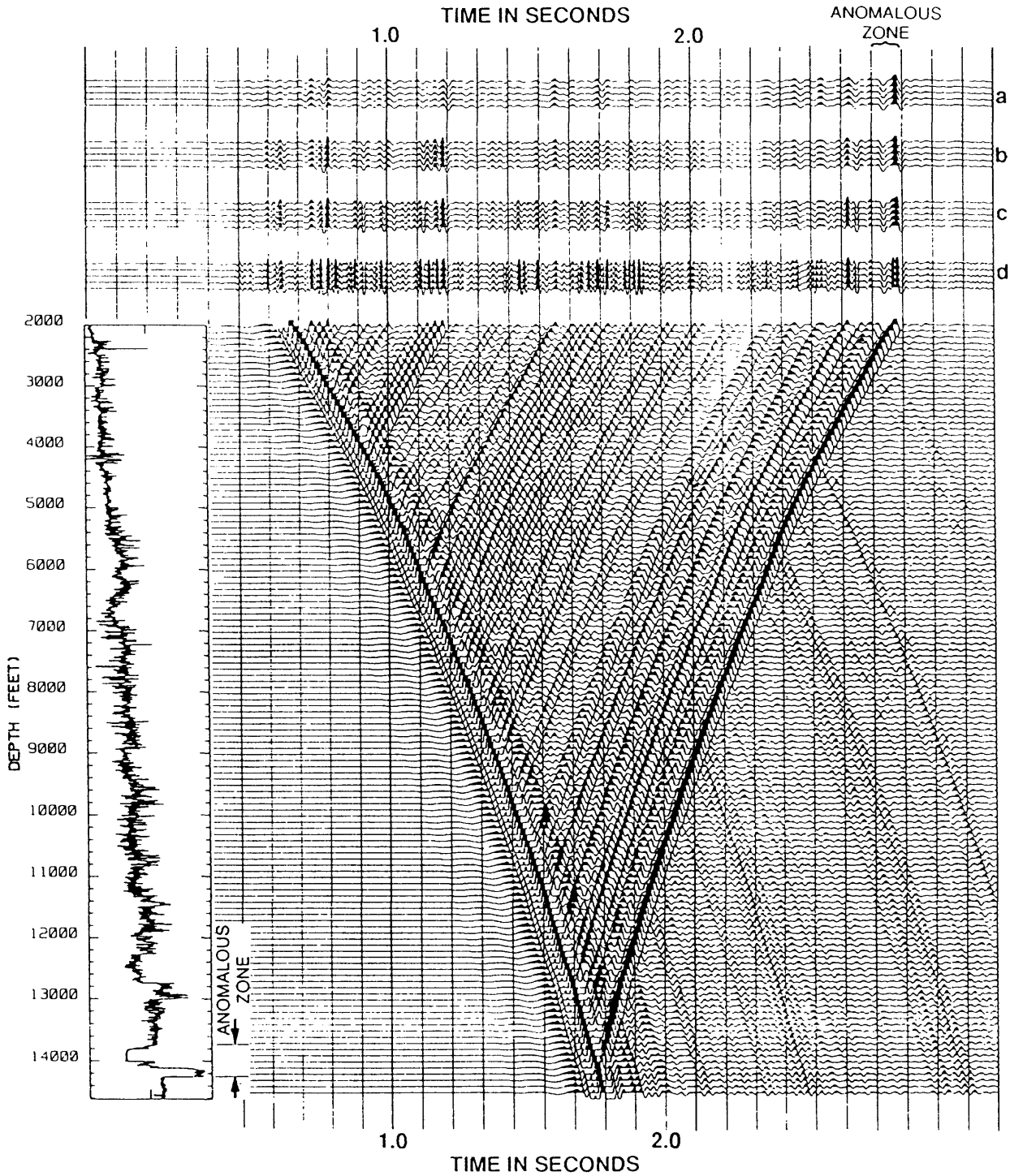

Fig. 9 Synthetic vertical profiles at OCS153A (EX975-1) using the linearly corrected sonic log. Synthetic seismograms (a, b, c, and d) are bandpass filtered at 6/10-32/42 Hz, 6/10-42/56 Hz, 6/10-50/68 Hz, and 6/10-68/96 Hz respectively. The letter **A** indicates the top of the anomaly and **B**, the bottom. The velocity log is plotted alongside the VSP.

seismic data (Figures 6, 7 and 9), which indicates that the top of the anomalous zone is a low impedance layer compared to the overlying layer. The actual seismic data strongly suggest that there exists an intermediate high-impedance layer within the anomalous zone. This arrangement is inferred from the small peak preceding the second trough. In order to estimate the acoustic property of the whole anomalous zone, an inversion method was applied to the stacked data.

The accuracy of inversion depends on variables such as:

1) The accuracy of the wavelet deconvolution,
2) Accurate estimates of reflection coefficients, and
3) Accurate estimates of low-frequency interval velocity.

Among these, the estimation of reflection coefficients was the most difficult in our case because the water depth was too shallow to estimate the water bottom reflection coefficients. Without water bottom reflection coefficients, we could not calibrate the seismic section to obtain meaningful reflection coefficients. Although less accurate, we used an amplitude decay curve shown in Figure 3 and the statistical estimate of the water bottom reflection coefficients vs water depth taken from the Blake Ridge area (appendix **A**) in a region off the southeastern Georgia embayment to estimate reflection coefficients. Figure 3 indicates that the maximum amplitude for the anomalous zone is about -24 db compared to the amplitude near water bottom. Using the approximated water bottom reflection coefficient of 0.4, expected in this water depth, and the amplitude decay curve of $T^{-1.93}$, the estimated reflection coefficients for the anomalous zone including polarity information is in the range of - 0.18.

With this reflection coefficient of -0.18 for the top of the anomalous zone and the average interval velocities, derived from the stacking velocities, the seismic section shown in Figure 7 was inverted for interval velocities using the inversion program supplied by Hampson & Russell Software Service, Ltd. We did not use density values for this inversion.

Figure 10 indicates that the top portion of the anomalous zone is a low-velocity layer of about 4 km/s velocity overlying a high-velocity layer of about 5.2 km/s. The 4 km/s velocity is similar to the average velocity of the upper part of the anomalous zone derived from the sonic log. All the analyses, polarity, amplitude, and velocity, are consistent with each other for the upper part of the anomaly. The key result of the inversion is the presence of a low-velocity layer with about 4 km/s interval velocity for the anomalous zone. However, the real velocity for the low-impedance layer could be higher than 4 km/s owing to the density contribution to the inversion, which we ignored.

The geometry of the anomalous body can be explained using the plots shown in Figures 11 and 12. Figure 11 is a portion of Figure 7 (wavelet and true-amplitude processed) and Figure 12 is an AGC section (processing sequence #1). Both sections show two prominent troughs (two prominent peaks in the reverse polarity sections) for the anomalous zone. The amplitude and spatial variation of the bottom trough negates the possiblity of peg-leg multiples or other interbed multiples being reponsible for the second trough. The top portion of Figure 12, which has a higher frequency content than the TA processed section (shown in Figure 11), clearly shows two peaks within the anomalous zone and that these peaks merge into a large single peak near CMPs 390 and 510. We interpret this to indicate that the anomalous zone has two distinct low-impedance layers separated by high-impedance layers. This seismic appearance was the major factor in leading us to conclude that the sonic log and density logs were in error.

In order to reinforce this interpretation, one-dimensional models with 6 layers were generated. The schematics of this model are shown in Figure 13 with seismic responses for various Ricker wavelets (15 Hz, 18 Hz, 20 Hz, and 25 Hz). The left portion of Figure 13 represents the seismic response for the central part of the anomaly and the right portion represents the seismic response for the edges of the anomaly, where two intermediate high-impedance layers thin out.

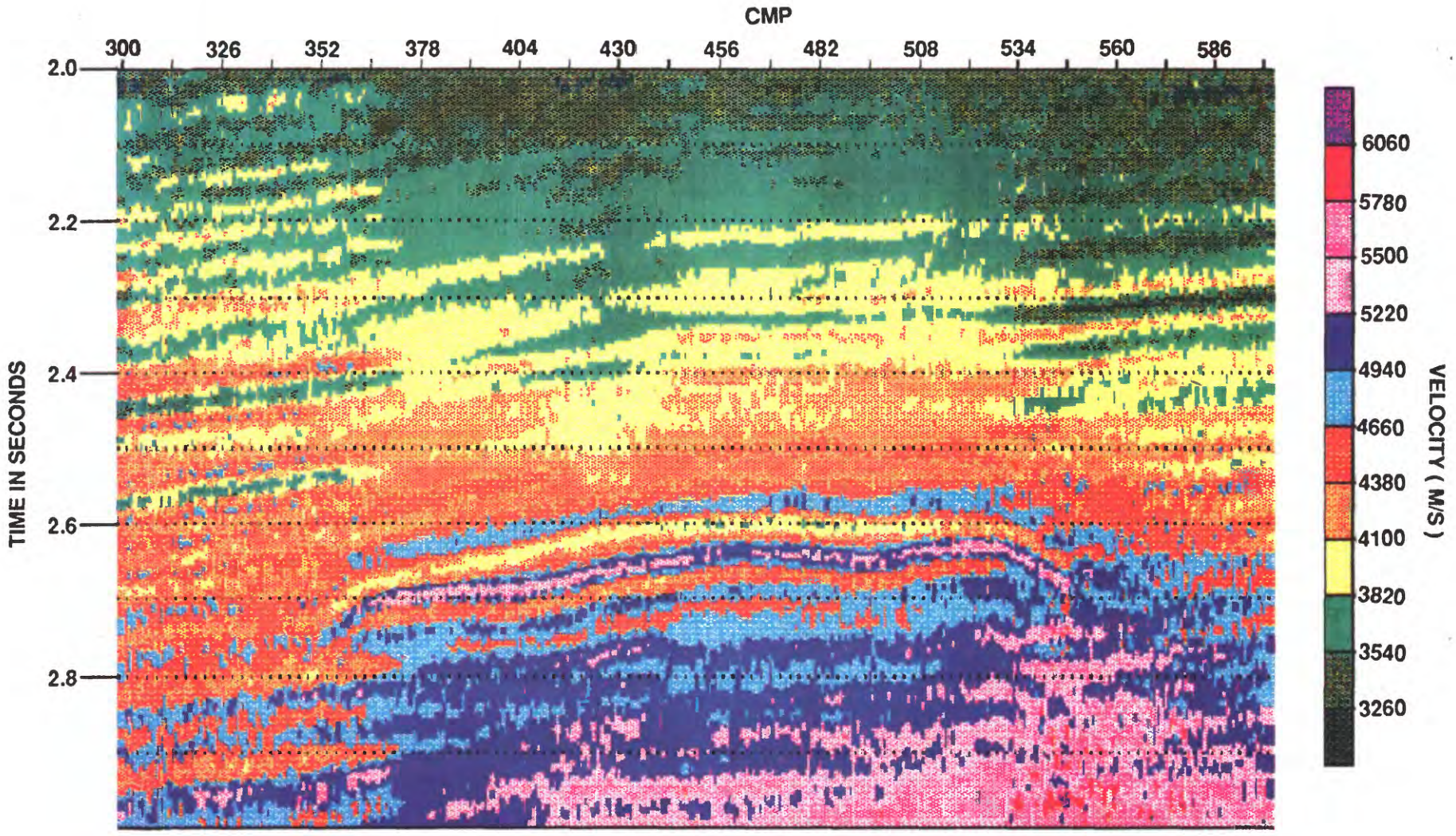

Figure 10 Interval velocities created by the linear inversion of the data shown in Figure 7. The inversion was performed using software from Hampson & Russell Software Service, Ltd. A high-velocity layer (about 5.2 km/s) is shown sandwiched between two low-velocity (about 4 km/s) layers at the top and bottom of the anomaly.

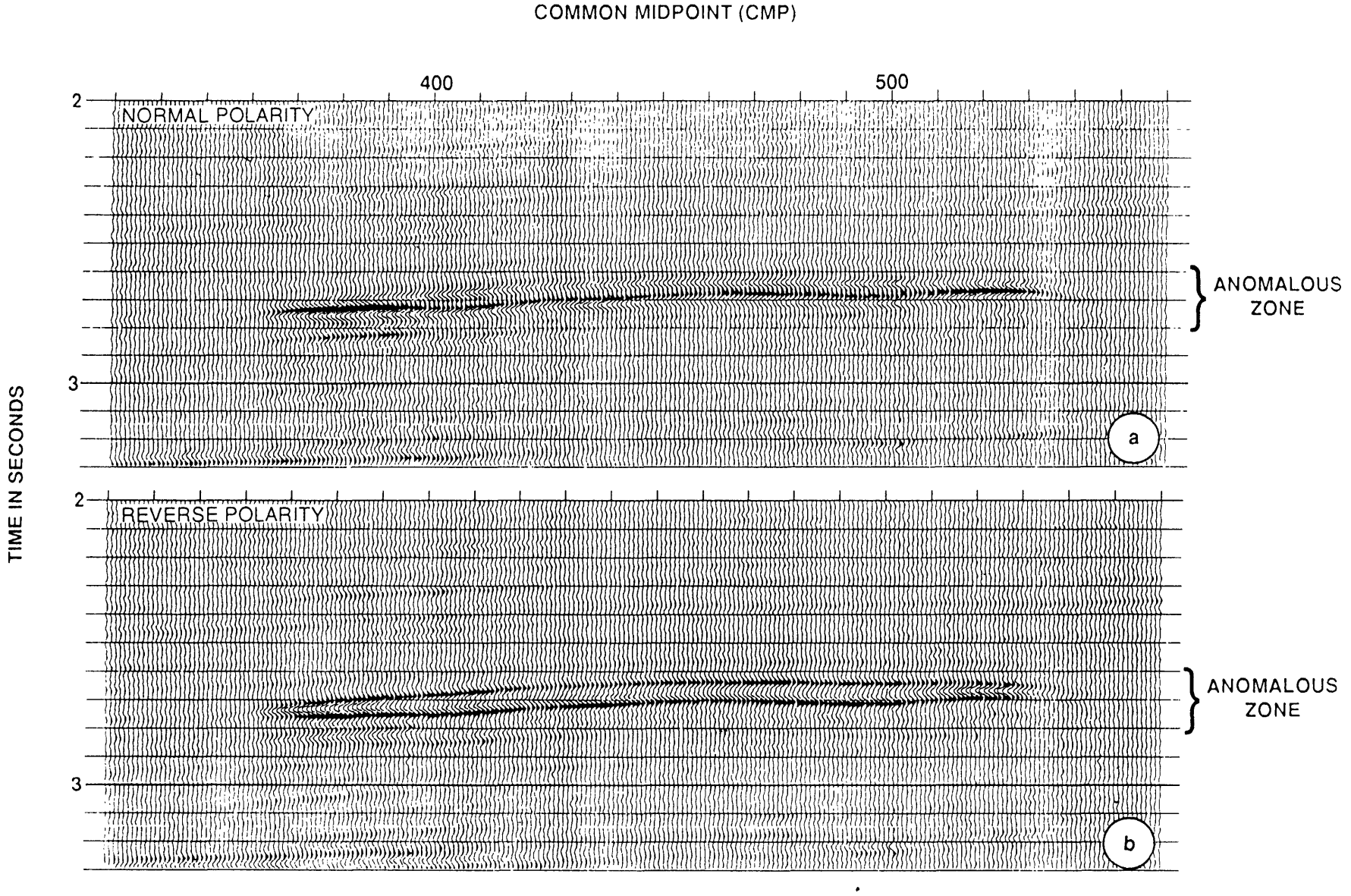

Fig. 11 Expanded view of the TA processed version of seismic profile 12 showing the anomalous zone in detail.
a) Normal Polarity Plot b) Reverse Polarity Plot

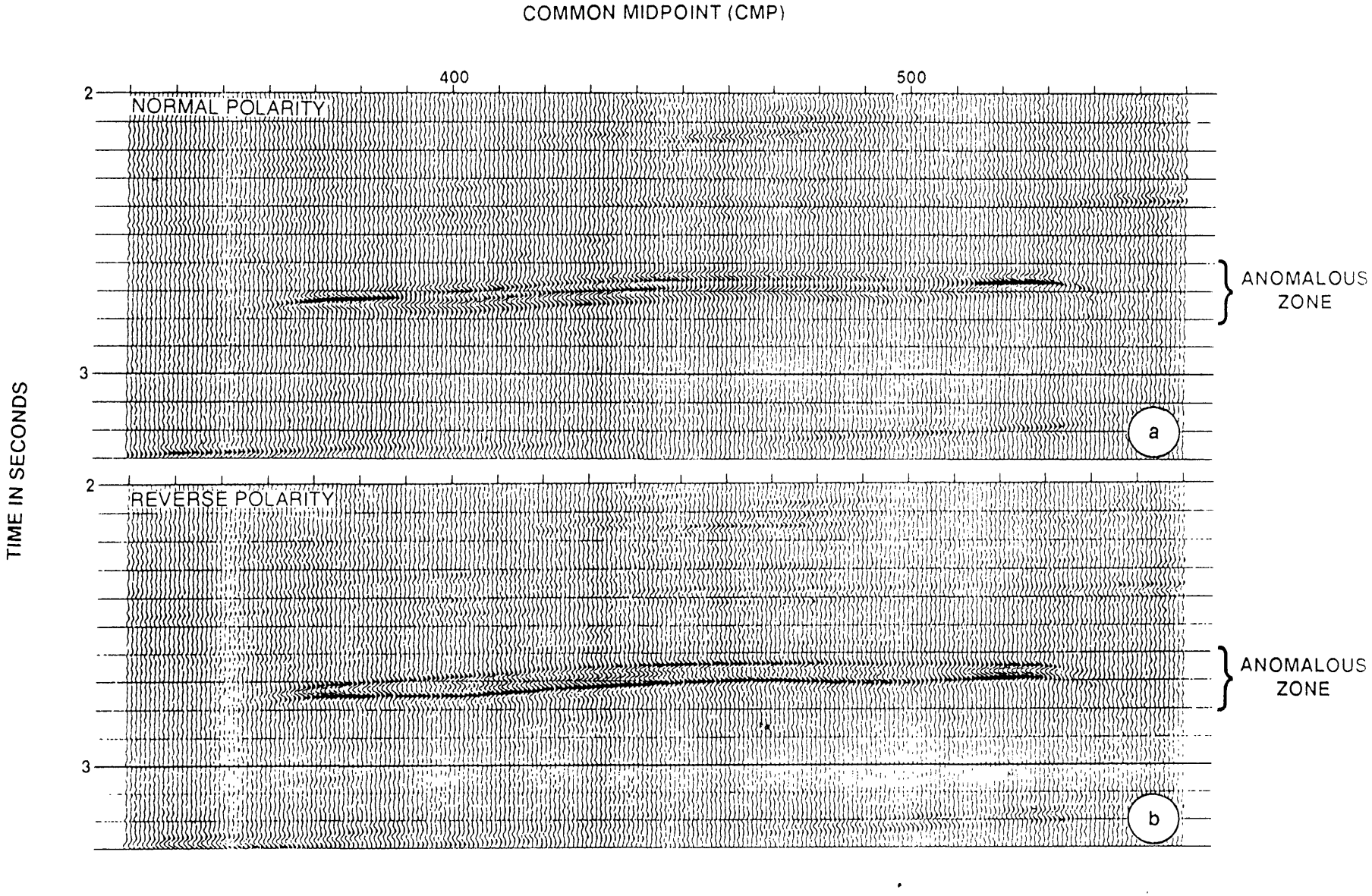

Fig. 12 Expanded view of the AGC processed version of seismic profile 12 showing the anomalous zone in detail.
a) Normal Polarity Plot b) Reverse Polarity Plot

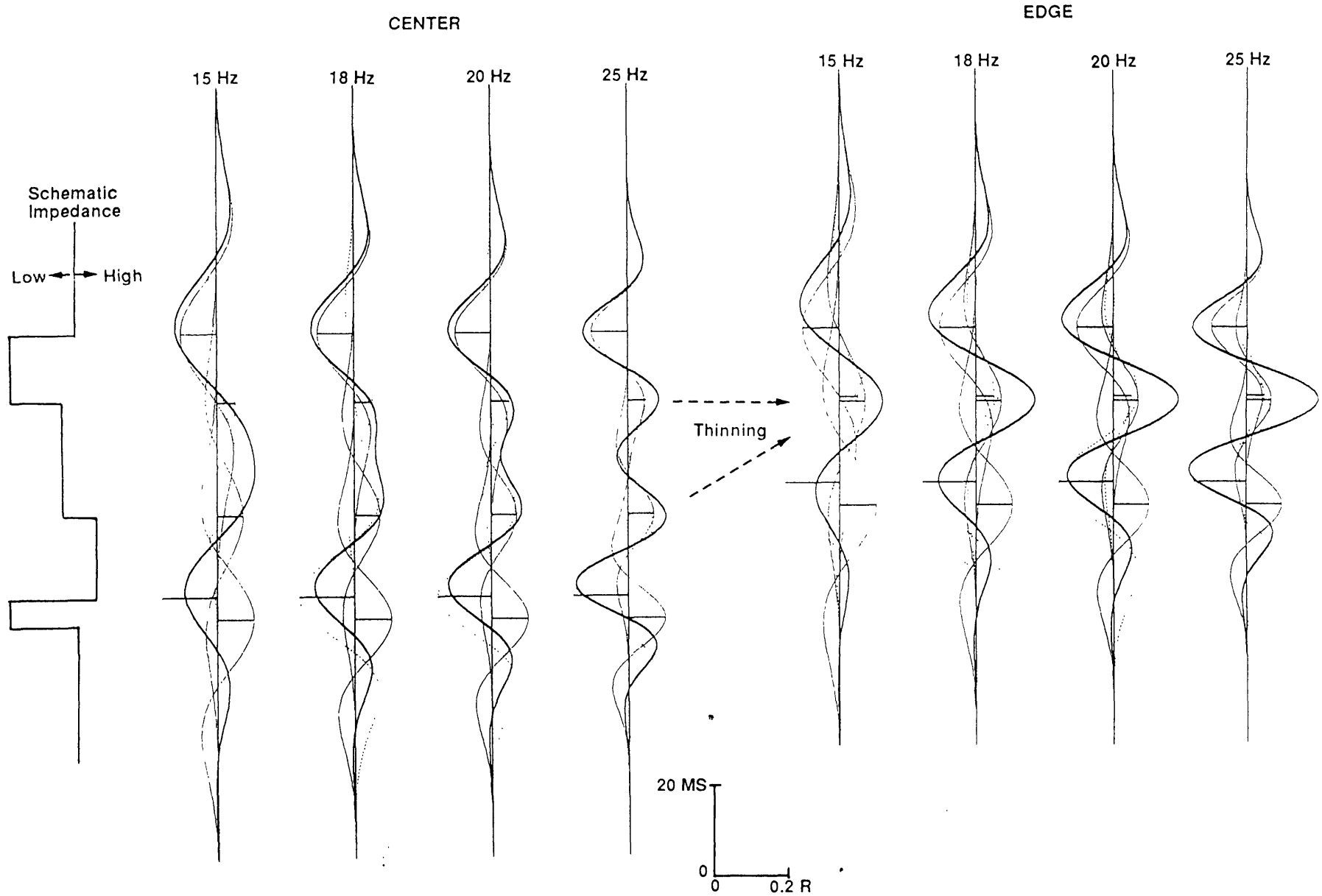

Fig. 13 One-dimensional model for the anomaly shown in Figures 11 and 12 using 15 Hz, 18 Hz, 20 Hz, and 25 Hz Ricker wavelets. Each spike represents the reflection coefficient from the acoustic boundary. Light solid and light dotted lines represent individual seismic responses from the boundary, and the heavy solid lines represent the total seismic response similar to that of the seismic section. A schematic one-dimensional model is shown at the far left side of the figure.

The response from the lower frequency part (18 Hz) corresponds to the seismic profile shown in Figure 11 and the higher frequency response (25 Hz) corresponds to the seismic profile shown in Figure 12. The overall wavelet shape and amplitude variations indicated in Figure 13 are well matched to the actual seismic profile.

Discussion

All the analyses indicate that the top and the bottom part of the anomalous zone are low-impedance layers with a low interval velocity of about 4 km/s. The inversion results shown in Figure 10 indicate that the interval velocity of the first low-impedance layer is about 4 km/s and the second low-impedance layer is about 4.2 km/s separated by a 5.2 km/s high-impedance layer. As mentioned previously, the density contribution to the seismic amplitude inversion was ignored. Thus the actual velocity of the low-impedance layers should be higher than shown in Figure 10 and the actual velocity for the high impedance should be lower than the one shown in Figure 10.

Because the anomalous zone is characterized by a low velocity compared to the surrounding rocks, its effect can be seen as a time anomaly in the seismic profile. The slight time sag of horizon **B-B'** in Figure 7 is due to the low velocity of the anomalous zone. The time sag is about 25 ms near CMP 500. If we assume that the time sag of 25 ms is solely due to the low velocity zone replacing high-velocity underlying rocks with an average velocity of 5.2 km/s, we can compute the average interval velocity of the anomalous zone by solving the following equation.

$$D/V - D/5.2 = 25/2 \text{ ms} \qquad (1)$$

where D is the thickness of the anomalous zone and V is the interval velocity. Using D = 100 m from the well-log information, the velocity is estimated as about 3.1 km /s. This is too low for the anomalous zone.

Figure 7 shows that we can observe a time high over the anomaly as well as a time sag underneath the anomaly. The time interval between horizons **A-A'** and **B-B'** in Figure 7 is plotted in Figure 14. If we assume that the linear approximation between CMP 350 and 550 corresponds to the regional time interval without the anomalous body, the total time delay from the anomalous body is about 50 ms for the central part of the anomaly. If we interpret the anomalous body as an intrusive body such as a salt intrusion, we can estimate the velocity of this anomaly by the following equation.

$$D / V = 50/2 \text{ ms.} \qquad (2)$$

This equation gives a 4 km/s average velocity for the anomalous zone. This velocity is slightly lower than, but closer to, the velocity estimated by the inversion method.

Based on the estimated velocities from Equations (1) and (2), the draping over the anomalous zone and diffractions at the edges, we prefer the interpretation that the anomaly is caused by an intrusive type body .

In computing interval velocities by Equations (1) and (2), we used the thickness of the anomalous body based on the well logs. However, the best estimate of the thickness using only observable quantities on seismic profile is much thicker than 100 m. Figure 13 provides the best fit between seismic and model. The total thickness of the anomalous zone is 63 ms in two-way time.

If we apply the average velocity based on the inversion, say 4.2 km/s, then the thickness is estimated as about 130 m, which is about 30 m thicker than the thickness determined from the well log. We cannot offer a plausible answer to this discrepancy at present.

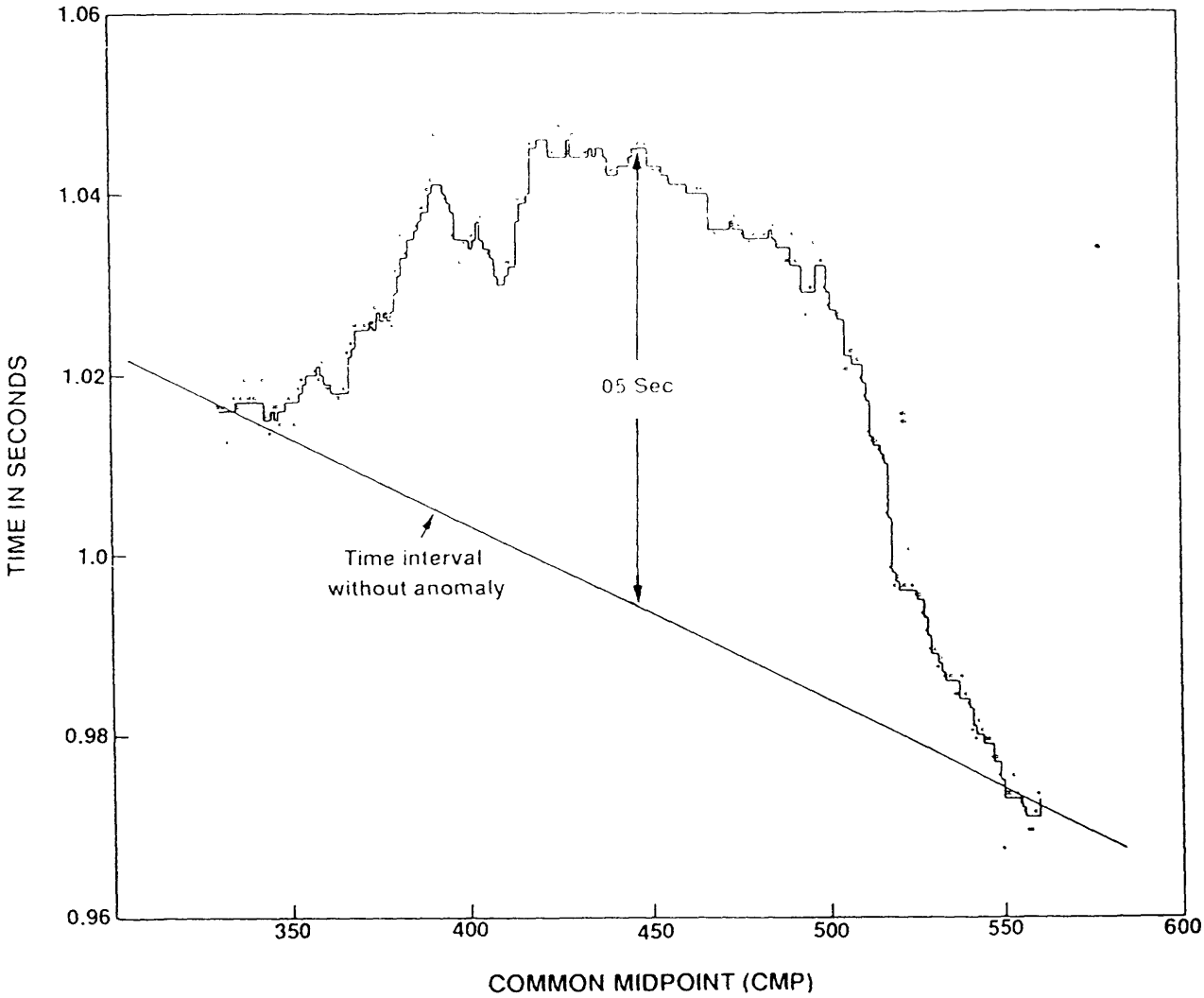

Fig. 14 Time interval surrounding the anomalous body shown in Figure 7. The time intervals were measured between horizon **A-A'** and **B-B'**. Base line indicates the regional time interval, in the absence of an anomaly. Each dot denotes an individual measurement at each CMP location and the solid line indicates the 3 point running median of individual measurements.

In order to constrain the lithological interpretation, the density of the anomalous body should be estimated. Seismic-inversion and stacking-velocity analysis indicate that the interval velocity of overlying rock is about 4.8 km/s. If we assume that the density of the overlying body is 2.55 g/cc, then the density of the top part of the anomaly can be estimated using the reflection coefficient of -0.18 and a velocity of about 4 km/s. This gives a density of the anomalous body of about 2.12 gr/cc, which is indicative of a salt body. Salt is inferred for this anomalous zone from the chloride values in the well log.

Conclusions

The following conclusions can be drawn from the detailed study of the anomalous seismic amplitude observed on the USGS line 12 seismic profile crossing the Georges Bank Basin.

1) The seismic response of the top of the anomaly is a strong trough with a reflection coefficient of -0.18 and the anomalous zone consists of two low-impedance layers separated by high-impedance layers which thin out laterally. The interpretation of the low impedance layers agrees with the interpretation of Anderson and Taylor (1981)
2) The anomalous body is characterized by a velocity of about 4 km/s and a density of 2.12 gr/cc.
3) The external seismic expression of the anomalous body such as diffractions, the draping of overlying layers over the anomalous body, and the time delay associated with the anomaly support the interpretation of a salt intrusion being responsible for the anomaly.
4) The lithologic interpretation based on the seismic profile matches well log information. But the thickness of the anomalous body is overestimated by 30 m (130 m vesus 100 m).
5) This case study indicates that seismic data contain ample information related to lithology. But only careful processing and analysis of seismic data can reveal the relevant information.

References

Anderson, R. C. and Taylor, D. J., 1981, Very high amplitude seismic anomaly in Georges Bank Trough, Atlantic continental margin: The American Association of Petroleum Geologists Bulletin, vol. 65, p. 133-144.

Backus, M. M., 1987, Amplitude versus offset: A review: Society of Exploration Geophysicists 57th annual international meeting and exposition, Oct. 11-15, New Orleans, Expanded abstracts, p. 359-364.

Emery, K. O., and Uchupi, E., 1972, Western North Atlantic Ocean, Topography, rocks, structure, water, life, and sediments: American Association of Petroleum Geologists, Memoir 17. 532p.

Gray, W. C., 1979, Variable norm deconvolution: Palo Alto, CA, Stanford University Ph.D. Thesis.

Jansa, L. F., and Wade, J. A., 1975, Geology of the continental margin off Nova Scotia and Newfoundland: Offshore geology of eastern Canada, v. 2, Regional Geology: Canada Geological Survey Paper 74-30, p. 51-105.

Lee, M. W., and Hutchinson, D. R., 1990, True-amplitude processing techniques for marine, deep crustal reflection seismic data: U.S. Geological Survey Bulletin 1897, 22 p.

Macknight, E. E., and Pena, M. J., 1988, Digital Log Processing System (DLPS) Users Manual (Release 5.2): CogniSeis Development, Manual, 517p.

Mattick, R. E. et al, 1975, Sediments, structural framework, petroleum potential, environmental conditions, and operational considerations of the United States North Atlantic outer continental shelf: U. S. Geological Survey Open-File Report 75-353, 179 p.

Poag, C. W. and Sevon, W. D., 1989, A record of Appalachian denudation in post-rift Mosozoic and Cenozoic sedimentary deposits of the U.S. middle Atlantic continental margin, in T. W. Gardner and W. D. Sevon, eds., Appalachian Geomorphology, Geomorphology, 2, p.119-157.

Schlee, J. S., et al, 1976, Regional geologic framework off northeastern United States: AAPG Bulletin, v. 60, p. 926-951

Schlee, J. S., et al, 1977, Petroleum geology on the United States Atlantic-Gulf of Mexico margins: Exploration and economics of the petroleum industry, v. 15: New York, Matthew Bender and Co., Inc.

Schlee, J. S., and Klitgord, K. D., 1981, Regional geology and geophysics in the vicinity of Georges Bank basin, in Schlee, J. S., ed., Summary of report of the sediments, structural framework, petroleum potential, and environmental conditions of the United States middle and northern continental margin area of proposed oil and gas lease sale no. 82: U. S. Geological Survey Open-File Report 81-1352, p. 17-36.

Sherwin, D. F., 1973, Scotian Shelf and Grand Banks: R. G. McCrossan, ed., Future petroleum provinces of Canada -- their geology and potential: Canadian Society of Petroleum Geologists Mem. 1, p. 519-559

Wyatt, K. D., 1981, Synthetic vertical seismic profiles: Geophysics, v. 46, p. 880-891

APPENDIX A

A relationship between the water-bottom reflection coefficient and water depth has been established in the Blake Ridge region, near the continental margin of southeastern United States. The water-bottom reflection coefficients were computed from 6 multichannel seismic profiles using the first-order water-bottom multiples. Each cross shown in Figure **A1** indicates an individual estimation of water-bottom reflection coefficient and the dotted line represents the linear regression line, where the regression equation is given by;

$$R = -5.36 * (T / 100) + .411$$

where,

R = Reflection coefficient

T = Two-way water depth in seconds

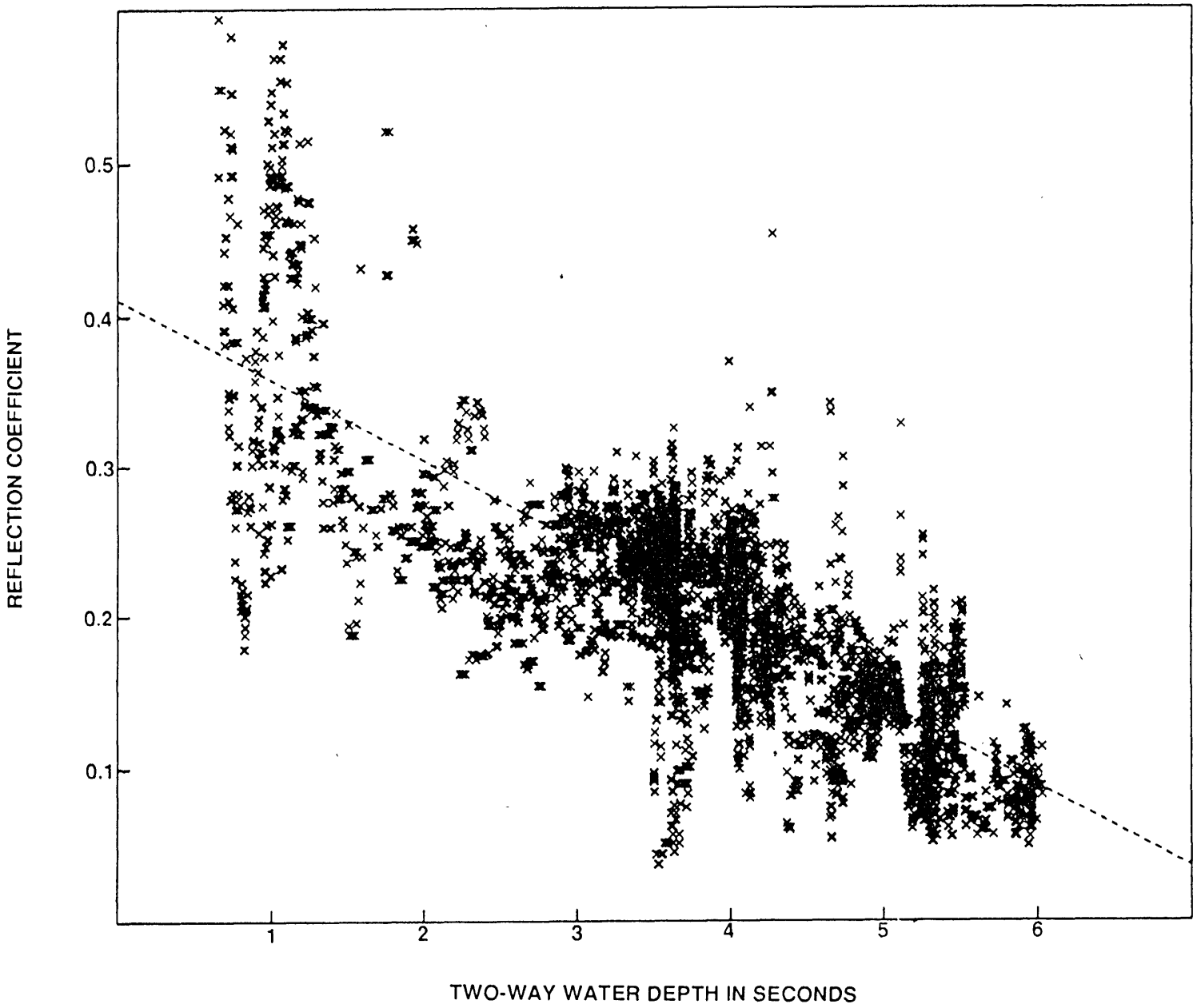

Fig. A1 A plot showing the relationship between the water-bottom reflection coefficients and water depths from the Blake Ridge area, near the continental margin off the southeastern United States. Each cross represents an individual measurement from 6 seismic profiles in the area. The solid line represents the linear regression line.